



Synthesis and evaluations of Fe₃O₄–TiO₂–Ag nanocomposites for photocatalytic degradation of 4-chlorophenol (4-CP): effect of Ag and Fe compositions

Amir Shojaie¹ · Moslem Fattahi¹ · Sahand Jorfi² · Bahram Ghasemi¹

Received: 31 October 2017 / Accepted: 23 April 2018 / Published online: 4 May 2018
© The Author(s) 2018

Abstract

This work reports the synthesis of nanocomposites of Fe₃O₄–TiO₂–Ag with different weight concentrations of iron (Fe) and silver (Ag) doped on TiO₂. The nanocomposites were prepared by a novel and facile ultrasonic-assisted hydrothermal method, and their effectiveness was evaluated for photocatalytic degradation. X-ray diffraction, scanning electron microscopy, Fourier transform infrared spectroscopy, and N₂ adsorption–desorption methods were performed to characterize the prepared catalysts. The photocatalytic activity of Fe₃O₄–TiO₂–Ag was studied by illumination of 4-chlorophenol (4-CP) in an aqueous solution under UV irradiation, which showed significant enhancement in the degradation of 4-CP compared to un-doped nano TiO₂. The maximum degradation of 97% in 165 min for Fe³⁺ and Ag⁺ with 0.3 and 2% wt. was observed. Furthermore, the stability and reusability of the synthesized catalysts were studied and demonstrated only 3% decrease in removal efficiency after five cycles.

Keywords Photocatalytic degradation · Fe–Ag doped TiO₂ · Hydrothermal synthesis · 4-Chlorophenol · UV irradiation

Introduction

The development of economy and industrialization, caused water contamination especially those contained organic dye and phenolic compounds to its toxic and harmful, has made people take it into a serious consideration [1–5]. 4-Chlorophenol (4-CP) is toxic and non-biodegradable, and is present in wastewater as by-products of pulp and paper, petrochemical industries, dyestuff, and pharmaceutical [6–9]. In recent years, titanium dioxide (TiO₂) has been extensively investigated as an environmental friendly and

clean photocatalyst [10–12]. TiO₂ has wide applications in wastewater treatment, water splitting hydrogen generation, solar cells, gas sensors, and air purification [13–15]. TiO₂ is a popular photocatalyst due to the good photocatalytic activity, low cost, non-toxicity, strong oxidizing potential, being inert, and stability for long time [10, 16–19]. It exists in four mineral forms including the anatase, rutile, brookite, and titanium dioxide (B) [20]. Phase transformation from amorphous to anatase occurred at 500 °C, and the transformation from anatase to rutile phase occurred at 700 °C. Complete rutile phase was formed at 900 °C with corresponding increase in the particle size [21]. Photocatalytic activity of TiO₂ has a relationship with its size, shape, surface area, morphology, and dimensionality [16]. However, utilizing TiO₂ has two drawbacks: first high energy band-gap (approximately 3.2 eV), which requires ultraviolet (UV) radiation for photo-induced activation. Another disadvantage is high electron (*e*[−])–hole (*h*⁺) recombination rate [3, 22, 23]. Considerable research and development works have been carried out to overcome the aforementioned limitations. In recent years, doping metals such as Fe, Ag, Cr, Sn, and Pt are the most suitable solution [2, 21, 24–26]. Tong et al. [27] studied on photocatalytic methyl orange degradation. The preparation of Fe³⁺-doped TiO₂ catalysts and

✉ Moslem Fattahi
fattahi@put.ac.ir

Amir Shojaie
amirsh9065016@yahoo.com

Sahand Jorfi
sahand369@yahoo.com

¹ Department of Chemical Engineering, Abadan Faculty of Petroleum Engineering, Petroleum University of Technology, Abadan, Iran

² Department of Environmental Health Engineering, School of Health, Ahvaz Jundishapur University of Medical Sciences, Ahvaz, Iran



their photocatalytic activity for methyl orange degradation were investigated in their report. Results showed that Fe^{3+} ions can be successfully incorporated into the crystal lattice of TiO_2 [27]. Jia et al. [5] synthesized $\text{Fe}_3\text{O}_4\text{-TiO}_2$ heterostructures through the co-precipitation method. In this work, the triple surface heterostructures, $\text{Ag@Fe}_3\text{O}_4\text{-TiO}_2$, were prepared by a chemical solution-deposition process. The photocatalytic activity of $\text{Fe}_3\text{O}_4\text{-TiO}_2$ was found to decrease due to increase in the rate of recombinations. Results investigated the composite coated with Ag metal ions, increasing its photocatalytic activity [5]. It is not easy to compare the results reported for doped semiconductor due to different experimental conditions and synthesis methods. The photocatalytic activity of the doped TiO_2 relies on the nature and concentration of the dopant ion [22]. The optimum weight concentrations of Fe and Ag dopant technique are widely used in different studies. In this work, the amount of Fe chosen from optimum concentration of different researches and the photo-reduction were preferred for the fabricated of Ag on $\text{Fe}_3\text{O}_4\text{-TiO}_2$.

In this study, the uniform nanocatalysts of $\text{Fe}_3\text{O}_4\text{-TiO}_2$ were synthesized by a facile hydrothermal method. Ag-doped $\text{Fe}_3\text{O}_4\text{-TiO}_2$ NCs were modified in silver acetate solution under UV light by a photochemical reduction technique. Then, the concentration effects of iron (Fe) and silver (Ag) doped on TiO_2 from the viewpoint of morphology and degradation rate were investigated. The prepared catalyst was characterized through the XRD, SEM, FTIR, and BET techniques. Besides, the photocatalytic activity of $\text{Fe}_3\text{O}_4\text{-TiO}_2\text{-Ag}$ was studied by illumination of 4-CP aqueous solution under UV irradiation, and the reaction kinetics of removal were considered.

Materials and methods

Materials

All the chemical materials, including titanium tetrabutoxide, $\text{Ti}(\text{OC}_4\text{H}_9\text{-}n)_4$ with purity of 98%, iron (III) nitrate [$\text{Fe}(\text{NO}_3)_3\cdot 9\text{H}_2\text{O}$, 99%] as the source of Fe, ethanol ($\text{C}_2\text{H}_5\text{OH}$, 99.7%), glacial acetic acid (CH_3COOH , 99.5%), sulfuric acid (H_2SO_4 , 98%), and silver acetate (CH_3COOAg) used in this study, were all analytical grade and purchased from the Merck company.

Catalyst preparation

Synthesis of $\text{Fe}_3\text{O}_4\text{-TiO}_2$ NCs

The synthesise procedure under magnetic stirring was as follow: 20 mL acetic acid was added dropwise to a flask containing 10 mL of $\text{Ti}(\text{OC}_4\text{H}_9\text{-}n)_4$ diluted in 30 mL

$\text{C}_2\text{H}_5\text{OH}$, followed by the addition of 1 mL H_2SO_4 and a specific amount of $\text{Fe}(\text{NO}_3)_3\cdot 9\text{H}_2\text{O}$ (0.05, 0.01, and 0.3% wt. of $\text{Fe}_3\text{O}_4\text{-TiO}_2$). Then, the obtained clear liquid was sonicated in an ultrasonic for 2 h, resulting in the formation of a milk-like solution which was further transferred into a stainless autoclave and kept at 453 K for 13 h. The resulting precipitates were separated from the mother liquor by centrifugation, washed thoroughly with distilled water and ethanol three times, respectively, and then dried at 373 K in oven for 12 h.

Synthesis of $\text{Fe}_3\text{O}_4\text{-TiO}_2\text{-Ag}$ NCs

For synthesizing of Ag loading (1.0 and 2.0% wt. Ag in $\text{Fe}_3\text{O}_4\text{-TiO}_2\text{-Ag}$), the composite suspension was prepared by mixing Fe-TiO_2 nanoparticles (0.5 g) with a specific amount of CH_3COOAg aqueous solution and 50 mL of deionized water. Then, the prepared solution was stirred for 1 h at room temperature and 3 h under UV irradiation, continuously. The $\text{Fe}_3\text{O}_4\text{-TiO}_2\text{-Ag}$ nanocomposites were separated from the reaction media by centrifugation, washed completely with distilled water and ethanol, and then dried at 373 K in oven for 12 h. Finally, the prepared catalysts were calcined at 773 K for 4 h. Overall, at different weight percentages of Fe and Ag, six catalyst samples were prepared and the details are presented in Table 1.

Characterization

The X-ray diffraction (XRD) patterns were observed on a X-ray diffractometer using a Cu target K_α ray ($\lambda = 0.15406$ nm) to determine the crystalline structure and phase of nanomaterials by scanning in angular range (2θ) from 20° to 80° (Philips, PW1730 diffractometer, Netherlands). The particle size and morphology of $\text{Fe}_3\text{O}_4\text{-TiO}_2\text{-Ag}$ NCs were studied with scanning electron microscopy (FESEM-TESCAN MIRA3, Kohoutovice, Czech Republic), which was equipped with an energy-dispersive spectroscopy (EDS). FTIR spectra were recorded between the wave number of 400 and 4000 cm^{-1} (Bruker,

Table 1 Synthesized catalysts at different conditions in this study

Catalyst sample	Weight concentration of Fe	Weight concentration of Ag
Sample-1	0.05	1
Sample-2	0.05	2
Sample-3	0.1	1
Sample-4	0.1	2
Sample-5	0.3	1
Sample-6	0.3	2

Model: VERTEX70, Germany). The specific surface area (BET method), specific pore volume, and average pore diameter (BJH method) were determined using nitrogen adsorption at 77 K (Model: BELSORP MINI 3, Czech Republic).

Experimental setup and procedure

The photocatalytic activity of $\text{Fe}_3\text{O}_4\text{-TiO}_2\text{-Ag}$ NCs with different operational conditions along with un-doped nano TiO_2 for degradation of 4-CP in aqueous solution was carried out using an experimental setup. Setup included rectangular cubic glass photoreactor by a total volume of 480 mL ($4\text{ cm} \times 4\text{ cm} \times 30\text{ cm}$) without the upper face, which was equipped with two 8 W UVC lamps. For each test, a specific amount of catalyst was suspended into a glass reactor containing 100 mL of the 4-CP with specific concentration. The pH of solution was adjusted with 0.1 M HCl or 0.1 NaOH. Then, the above solution was stirred in the dark medium for 60 min to attain the adsorption–desorption equilibrium for 4-CP and dissolved oxygen on the surface of $\text{Fe}_3\text{O}_4\text{-TiO}_2\text{-Ag}$ NCs. After every given irradiation time, the mixture was sampled and centrifuged for 14 min at a rate of 11,000 rpm. The concentration of 4-CP in each test was determined through a UV–Vis spectrophotometer (Hach, DR 5000, USA) at $\lambda_{\text{max}} = 279\text{ nm}$. Removal was analyzed through the initial and final 4-CP concentrations according to following equation:

$$\text{Removal}(\%) = \frac{(C_0 - C_t)}{C_0} \times 100, \quad (1)$$

where C_0 is the initial concentration of 4-CP (mg/L) and C_t is the concentration of 4-CP (mg/L) at specified reaction time t (min).

Results and discussion

XRD analysis

X-ray diffraction was used to confirm the phase purity and crystallinity of the catalysts. The XRD patterns of samples containing different Fe and Ag contents are shown in Fig. 1. All samples consist of anatase as the unique phase. The peaks at scattering angles of 25.4° , 37.9° , 48.2° , 54° , 55.2° , and 62.9° are well supported with the JCPDS 21–1272, and correspond to the reflections from the (101), (004), (200), (105), (211), and (204) crystal planes, respectively. XRD patterns indicate that the crystal structure of TiO_2 remains unchanged after sensitization process, as reported in similar work [28]. The identified peaks located at 44.6° (400), 54° (422), and 62.8° (440) were attributed to Fe_3O_4 diffractions (JCPDS 65–3107) [29]. When Ag^+ ions are incorporated

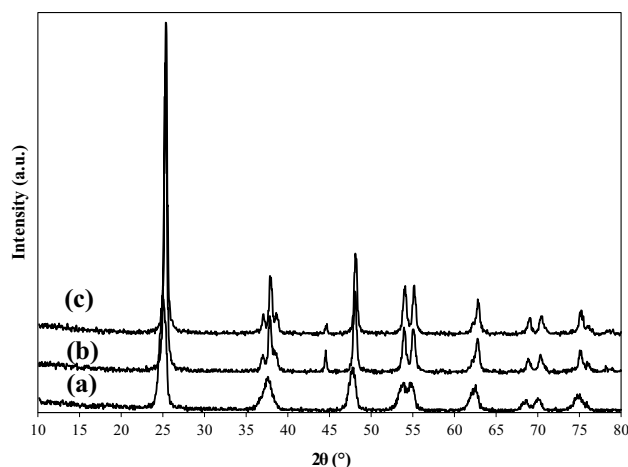


Fig. 1 XRD pattern of **a** sample-1, **b** sample-3, and **c** sample-6

into crystal lattice of $\text{Fe}_3\text{O}_4\text{-TiO}_2$ NCs, the peaks are found at 38.7° (111), 44.5° (200), and 62.9° (220) that confirmed the JCPDS 04–0783 [5, 22, 27, 30, 31]. After the addition of Fe species, the crystallinity of the $\text{Fe}_3\text{O}_4\text{-TiO}_2$ nanocomposites changed and was confirmed to be more addition of Fe amount that has great effect on the crystallinity intensity of the TiO_2 . The characteristic diffraction peaks corresponding to the anatase phase of TiO_2 remained unchanged in all samples without any peak shifting. Furthermore, the existence of new diffraction peaks of Fe_3O_4 was not identified, suggesting that the low loading of Fe_3O_4 might be dispersed well on the surface of the TiO_2 . The average crystallite domain sizes were calculated using the Scherrer equation from the fitting of the (101) peak corresponding to the anatase ($2\theta = 25.4^\circ$) [32–34]. The calculated average crystallite sizes for samples (a), (b), and (c) were 23.2, 19.2, and 16.8 nm, respectively. All samples have the same peaks, nearly; however, the average crystallite size of sample (c) is lower than that of other samples. Figure 1 does not show all peaks that satisfy Fe and Ag, due to their lower concentration (i.e., below the detection limit of the XRD).

FESEM and EDX analysis

Figure 2 shows the FESEM images of some samples which were prepared by a novel and facile ultrasonic-assisted hydrothermal method with mainly sphere-like shape. It is obvious that the Fe and Ag are successfully doped on the surface of TiO_2 . The size of particles varies from 12 to 50 nm, which represents that a particle is formed from many crystals. According to the literature, doping of Fe and Ag caused grain growth, which is restrained during the hydrothermal, and decreases the crystal size of TiO_2 (Degussa P25) [27, 35]. These phenomena may prevent particle agglomeration, forming well-defined nanocrystalline



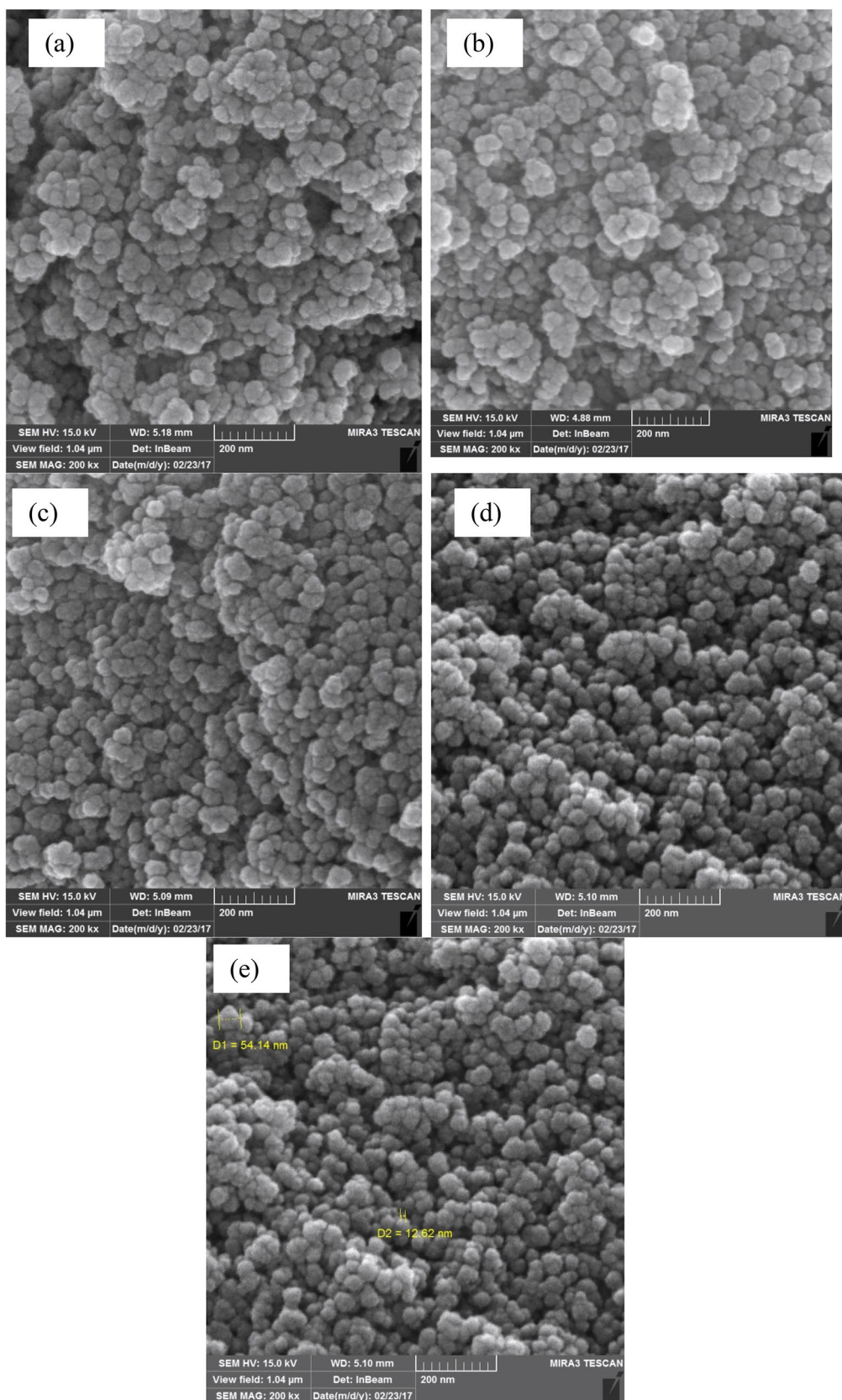


Fig. 2 Typical FESEM images of catalyst **a** sample-2, **b** sample-3, **c** sample-4, **d** sample-6, and **e** particle size of sample-6

powders with high surface area [26]. As shown in Fig. 2, the sample morphologies have no evident differences and all samples consist of spherical particle sizes below 50 nm. However, as the Fe and Ag contents increased to 0.3 and 2, respectively, it can be seen that the aggregation phenomenon occurred and many nanoparticles transformed into obviously bigger nanoparticles. Moreover, EDX results (Fig. 3) reveal that $\text{Fe}_3\text{O}_4\text{-TiO}_2\text{-Ag}$ is composed of Ti, O, Ag, and Fe elements, which was confirmed to the XRD results. According to Table 2, the experiment evaluated the weight percentage of Fe and Ag in sample-2 similar to the theoretical ones, which confirms that doping is perfect and complete through this condition.

FTIR analysis

FTIR analyses using KBr as reference show the characteristic peaks. FTIR spectra of $\text{Fe}_3\text{O}_4\text{-TiO}_2\text{-Ag}$ NCs (Fig. 4) showed the peaks corresponding to stretching vibrations of O–H groups on the catalyst surface and bending vibrations of water adsorbed on the surface around 3350–3450 and 1620–1635 cm^{-1} , respectively. Moreover, the $\sim 600\text{ cm}^{-1}$ band was associated with the Ti–O–Ti stretching vibration, which has been shifted to the lower wavelength as the addition of Fe^{3+} and Ag^+ ions. The peak at 1113 cm^{-1} was described by the C–H vibration of the acetate ion [3, 6, 36, 37]. The $\text{Fe}_3\text{O}_4\text{-TiO}_2\text{-Ag}$ NCs by observing a peak at $\sim 1080\text{ cm}^{-1}$ of the Fe_3O_4 along with the peaks of Ti–O–Ti ($\sim 600\text{ cm}^{-1}$) and the O–H vibrations ($\sim 3400\text{ cm}^{-1}$) confirm the formation of products, which corresponded to the open literature [36]. Almost all samples have the same results of FTIR.

Table 2 Quantitative element results from EDX technique

% wt.	Element	Sample-2	Sample-3	Sample-4	Sample-6
Evaluated	O	56.68	48.18	60.50	56.74
	Ti	41.40	50.97	39.07	42.12
	Fe	0.09	0.11	0.11	0.11
	Ag	1.82	0.73	0.33	1.03
Theory	O	–	–	–	–
	Ti	–	–	–	–
	Fe	0.05	0.1	0.1	0.3
	Ag	2	1	2	2

BET analysis

N_2 adsorption–desorption measurements reveal that nanoporous structure of catalyst was present for all samples. It was observed from Fig. 5 that the prepared samples possess mesoporous surface as the isotherms are of type IV [21, 38]. Using the Barrett–Joyner–Halenda model, the pore distribution of the nanocomposites is centered at 20 nm.

The average pore diameter from adsorption branch is 14.02 nm for sample-2 and sample-6. S_{BET} of nanospherical structure was estimated to be 44.60 and 43.62 m^2/g from adsorption curve. Table 3 shows that Fe and Ag loading led to an increase in the BET surface area and decreased its mean pore size diameter of the catalyst. This fact observed due to the obstacle of TiO_2 pores by metal oxidic species can take place, as their interactions with the support, which may be physical or chemical adsorption [38].

In our previous work, the optimum values of Fe and Ag were chosen as 0.3 and 2% wt. in which the $\text{Fe}_3\text{O}_4\text{-TiO}_2\text{-Ag}$

Fig. 3 EDX analysis of the sample-6

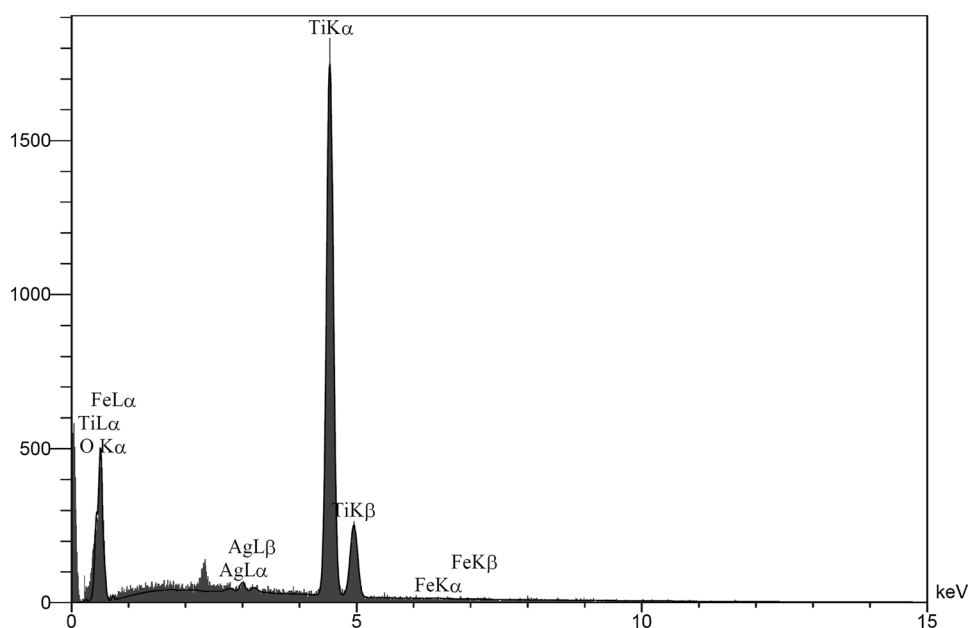
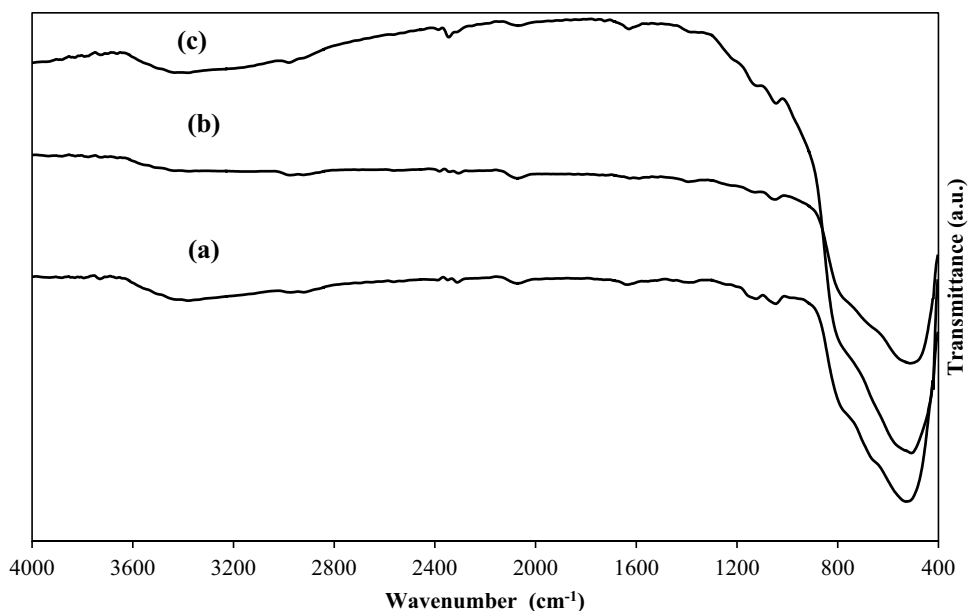


Fig. 4 FTIR spectra of the **a** sample-2, **b** sample-3, and **c** sample-6



photocatalyst showed considerable enhancement in the degradation of 4-CP compared to bare nano TiO₂ [39]. The introduction of the Fe and Ag loading led to an increase in the BET surface area and reduced its mean pore size diameter of the catalyst compared to the bare TiO₂ [39].

Photocatalytic activity

The photocatalytic activities of the Fe- and Ag-loaded samples for 4-CP decomposition were compared with un-doped TiO₂ (P25) under UV irradiation. The photocatalytic activity tests were performed in Fig. 6 at conditions including the pH = 3, irradiation time = 120 min, 4-CP concentration = 30 mg/L, and catalyst dosage of 1 g/L. According to Fig. 6, sample-6 was chosen as desired catalyst. According to Fig. 2, for sample-6, the Fe and Ag were distributed very well on TiO₂ in comparison to other samples. Besides, the crystal size of this sample was lower than others. Then, the operation conditions were optimized and removal efficiency increased to 97%. Table 4 also presents the reusability of the prepared nanocomposite after recycling. The photocatalytic degradation of Fe₃O₄-TiO₂-Ag NCs still maintained 94% efficiency, even after five cycles. In our previous work [40] under UV and solar irradiations, some nanocomposites exhibited higher photocatalytic efficiency compared to the bare TiO₂ (around 20 to 40%), which demonstrated the benefits of the nanocomposites in TiO₂-based photocatalytic systems.

Mechanism of 4-CP photocatalytic degradation

When UV light falls on the surface of Fe₃O₄-TiO₂-Ag, photo-generated electrons and holes are generated. Fe³⁺ ions can

act as electron and hole traps, hence forming Fe²⁺ and Fe⁴⁺ ions, which are less stable compared to Fe³⁺ ions. So, tends to return to Fe³⁺. This leads to the generation of OH· radical and O₂ anion [27, 34, 41].

Although the Ag Fermi energy level is lower than the conduction band of TiO₂, the oscillation hot electron around Ag is excited to higher energy level. So it could transfer to conduction band of TiO₂ by hot electron injection, furthermore these electrons were used to generate free radicals which enhances the photocatalytic activity [14, 42].

The photocatalytic reaction generally includes photo-excitation, charge separation and migration, and surface oxidation–reduction reactions [43]. The reactive species generated during illumination of photocatalysts are h⁺, OH⁻, and O₂⁻. To understand the mechanism of Fe and Ag for degradation 4-CP, it is necessary to detect which reactive species plays a major role in the photocatalytic degradation process. According to the results of the intermediate analysis and considering the degradation pathways suggested by existing literature studies [44–46], among the different active species, the OH· radical has been reported as the most important active species in the photocatalytic oxidation process. Since the OH· radicals are electrophilic and OH groups have electron-donating character, the OH· radicals attack the para and ortho positions of the benzene ring [40].

The schematic of pollutant oxidation removal through the TiO₂ are illustrated in Fig. 7. The beneficial effect of Fe³⁺ may be explained by considering the formation of Fe²⁺ species by means of a transfer of photo-generated electrons from TiO₂ to Fe³⁺ [Eq. (3)]. According to the crystal field theory, Fe²⁺ is relatively unstable due to the loss of d⁵ (half-filled high spin) electronic configuration and tends to return to Fe³⁺ (d⁵). Subsequently Fe²⁺ could be oxidized to Fe³⁺ by transferring electrons to absorbed O₂ on the surface of TiO₂ [Eq. (5)]. The

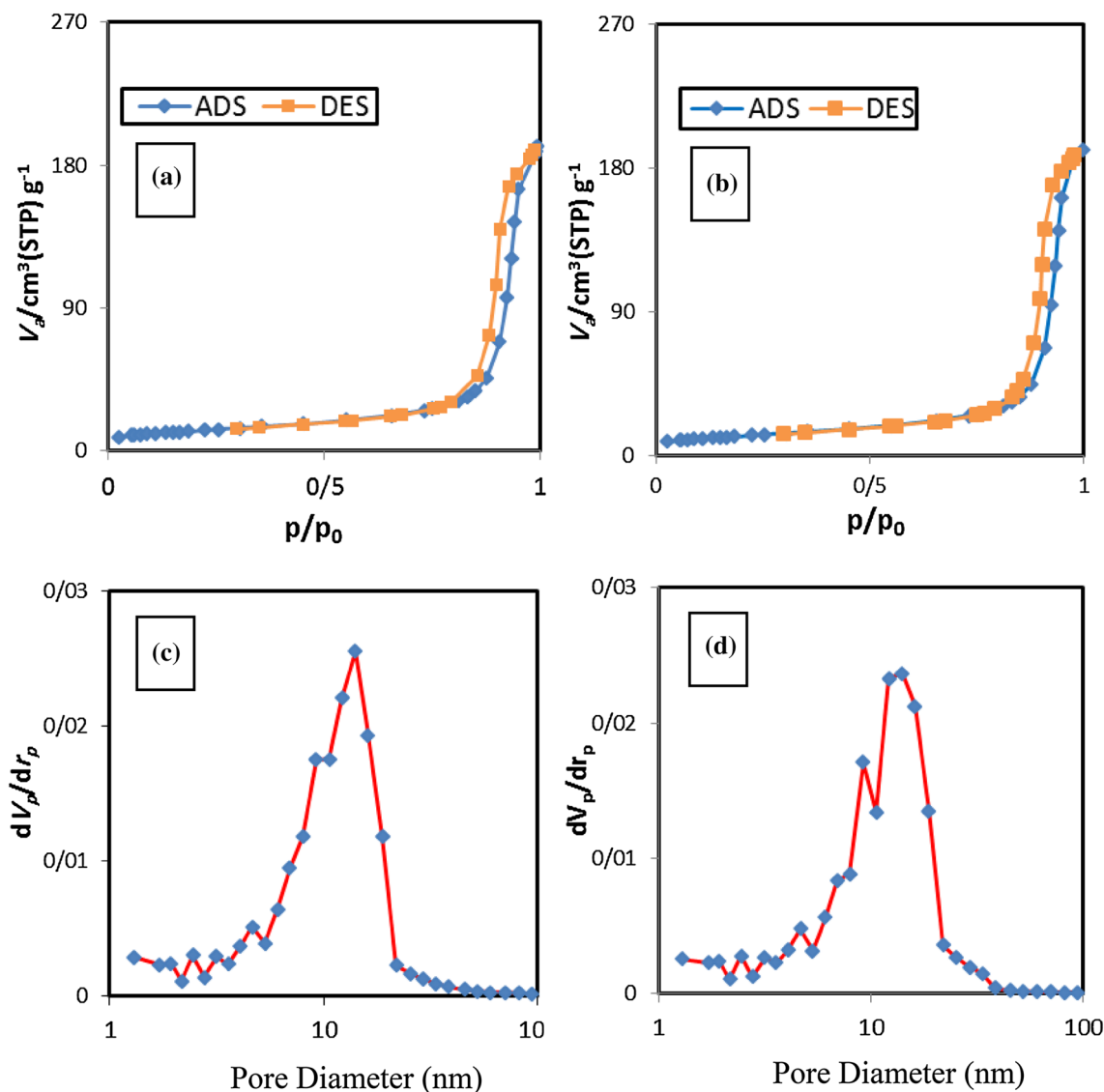


Fig. 5 a and b N₂ adsorption–desorption isotherms. c and d Macro pore size distribution plots of sample-2 and sample-6

Table 3 Properties of as-prepared sample-2 and sample-6 nanocomposites

Catalysts	S _{BET} (m ² /g)	BJH total volume (cm ³ /g)	BJH average pore size (nm)
Sample-2	44.60	0.300	14.02
Sample-6	43.62	0.296	14.02

Fe²⁺/Fe³⁺ energy level lies close to Ti³⁺/Ti⁴⁺ level. As a consequence of this proximity, the trapped electron in Fe²⁺ can also be easily transferred to a neighboring surface Ti⁴⁺ [Eq. (6)], which then leads to interfacial electron transfer. That is to say, Fe³⁺ can be an effective electron trap in anatase phase. Meanwhile, Fe³⁺ can also serve as hole trap [Eq. (12)] due to the

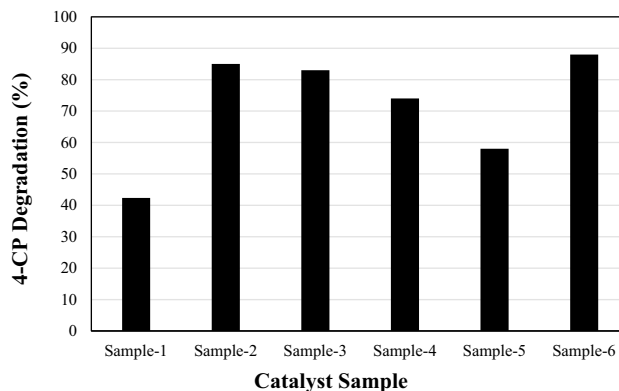
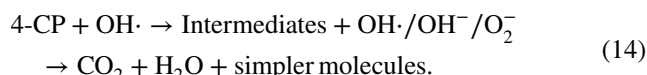
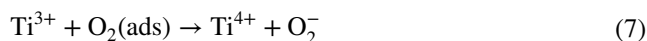
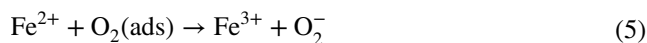


Fig. 6 Degradation results of different synthesized catalysts

energy level for $\text{Fe}^{3+}/\text{Fe}^{4+}$ above the valence band edge (E_{vb}) of anatase TiO_2 . The trapped hole embodied in Fe^{4+} has longer lifetime because of the immobilized electron in Fe^{2+} . Therefore, Fe^{3+} can act as both hole and electron traps, according to the following reactions [3, 5, 17, 47–49]:



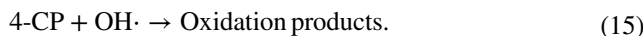
The conductive band electron further reacts with adsorbed O_2 to form O_2^- , while Fe^{4+} reacts with surface hydroxyl group to produce hydroxyl radical. Thus, 4-CP was photo-degraded even under the UV irradiation [Eq. (14)]. Besides, a decrease in the semicircle diameter of the titanium nanocomposites compared to the bare TiO_2 demonstrated a reduction in the resistance of interfacial charge transfer, leading to fast electron transfer and effective separation of photo-induced charge carriers. This phenomenon was related to very good conductivity properties of doped materials and the $\pi-d$ junction between the doped material and titanium which impressively facilitated the mobility of the electron and through charge separation, preventing the recombination of electrons and holes [40].

Table 4 Optimal conditions and reusability of catalyst with RSM and experimental ones

Reusability	pH	Time (min)	C_1 (mg/L)	C_{cat} (g/L)	Removal (%)
1	4.86	165	40.4	1.5	97.12
2	4.86	165	40.4	1.5	98.10
3	4.86	165	40.4	1.5	99.57
4	4.86	165	40.4	1.5	97.85
5	4.86	165	40.4	1.5	93.94

Kinetics of 4-CP photocatalytic degradation

Experimental studies were carried out at optimum conditions, pH = 4.86, catalyst dosage of 1.5 g/L, and 4-CP concentrations of 40.4 mg/L, to determine the degradation kinetic mechanism. The reactor was stirred by magnetic stirrer to complete photo-degradation process. Samples were taken from one reactor at 30, 60, 90, 120, 150, and 180 min after initiation of reaction. The models widely used are zero-, pseudo-first-, and second-order kinetic models. The degradation of 4-CP can be shown as follows:



Because $\text{OH}\cdot$ is a very reactive free radical, it does not accumulate in the reactor and its concentration is chosen as a steady-state value [50–52]. Pseudo-first-order kinetic respect to the concentration of the 4-CP is shown below:

$$\frac{d[4\text{-CP}]}{dt} = K_{\text{obs}}[4\text{-CP}][\text{OH}\cdot]. \quad (16)$$

Since $[\text{OH}\cdot]$ is constant at steady state, $K_{\text{obs}}[\text{OH}\cdot]$ is equal to K_{app} , where K_{obs} and K_{app} are absolute and apparent rate constants, respectively [53]. Equation (16) can be written as follows:

$$\frac{d[4\text{-CP}]}{dt} = K_{\text{app}}[4\text{-CP}]. \quad (17)$$

With integration of above equation, we have first-order kinetic equation:

$$\text{Ln} \frac{[4\text{-CP}]_0}{[4\text{-CP}]_t} = K_{\text{app}}t, \quad (18)$$

where $[4\text{-CP}]_0$ and $[4\text{-CP}]_t$ are the concentrations of 4-CP at the beginning and time t , respectively. The second-order kinetic equation is given as:

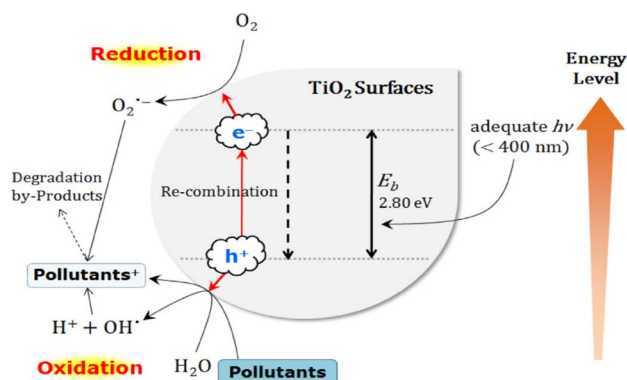


Fig. 7 Schematic illustration on removal of pollutants by the formation of photo-induced charge carriers (e/h^+) in a semiconductor TiO_2 particle surfaces [48]

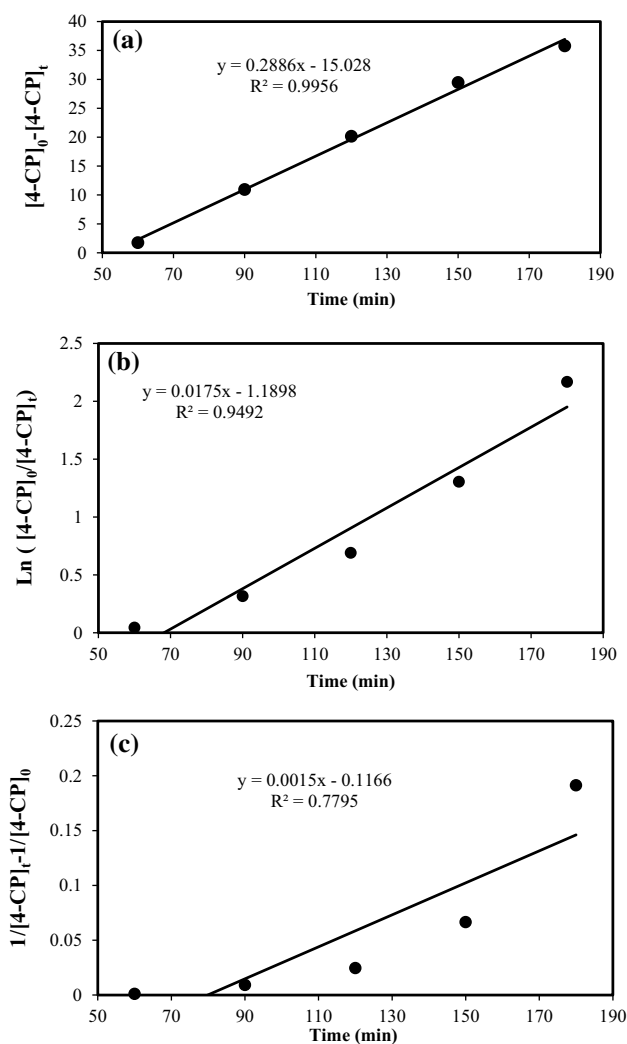


Fig. 8 **a** Zero-, **b** pseudo-first-, and **c** pseudo-second-order kinetic modeling of 4-CP removal

$$\frac{1}{[4-CP]_t} - \frac{1}{[4-CP]_0} = K_{app}t. \quad (19)$$

The zero-order kinetic equation can be written as follows:

$$[4-CP]_0 - [4-CP]_t = K_{app}t. \quad (20)$$

Modeling of 4-CP removal by zero-, pseudo-first-, and pseudo-second-order equation is shown in Fig. 8, respectively.

The correlation coefficient for the 4-CP removal kinetics of zero, pseudo-first, and second order was obtained 0.9956, 0.9499, and 0.7795, respectively. So, 4-CP degradation follows the zero-order kinetic models.

Conclusions

Nanocomposites of Fe_3O_4 - TiO_2 -Ag with different weight concentrations of iron (Fe) and silver (Ag) doped TiO_2 were synthesized in this investigation. The synthesized catalysts were characterized which confirmed that the average nanosphere size was from 12 to 50 nm and Ag is well dispersed on to Fe_3O_4 - TiO_2 . Furthermore, the Fe_3O_4 magnetic core facilitates the convenient recovery of the catalyst by applying an external magnetic field. Fe^{3+} can be easily integrated into the crystal lattice of TiO_2 and reduced recombination of photo-electrons. Silver nanoparticles combine with semiconductor, which promotes the separation of charges, produces more photo-generated charges in Fe_3O_4 - TiO_2 -Ag, and enhances bandgap absorption of TiO_2 .

According to characterization and primary photocatalytic activity tests, the catalyst with 88% degradation was chosen as the desired catalyst. Then, the operation conditions were optimized and removal efficiency increased to 97%. The most interesting feature from an application point of view is the combination of its photocatalytic response and the possibility to easily extract the photocatalyst by the deposition method. Furthermore, maximum degradation of 4-CP for the optimal conditions is 97% and photocatalytic degradation of Fe_3O_4 - TiO_2 -Ag NCs still maintains 94% efficiency, after five cycle recovery. Besides, 4-CP degradation kinetic rate was considered in which the degradation follows the zero-order kinetic.

Open Access This article is distributed under the terms of the Creative Commons Attribution 4.0 International License (<http://creativecommons.org/licenses/by/4.0/>), which permits unrestricted use, distribution, and reproduction in any medium, provided you give appropriate credit to the original author(s) and the source, provide a link to the Creative Commons license, and indicate if changes were made.

References

1. Mazloomi Tabaei HS, Kazemeini M, Fattahi M (2012) Preparation and characterization of visible light sensitive nano titanium dioxide photocatalyst. *Sci Iran* 19:1626–1631
2. Safari M, Talebi R, Rostami MH, Nikazar M, Dadvar M (2014) Synthesis of iron-doped TiO_2 for degradation of reactive orange16. *J Environ Health Sci Eng* 12(19):1–8
3. Mesgari Z, Gharagozlu M, Khosravi A, Gharanjig K (2012) Spectrophotometric studies of visible light induced photocatalytic degradation of methyl orange using phthalocyanine-modified Fe-doped TiO_2 nanocrystals. *Spectrochim Acta Part A Mol Biomol Spectrosc* 92:148–153



- Pazoki M, Parsa M, Farhadpour R (2016) Removal of the hormones dexamethasone (DXM) by Ag doped on TiO₂ photocatalysis. *J Environ Chem Eng* 4:4426–4434
- Jia X, Dai R, Lian D, Han S, Wu X, Song H (2017) Facile synthesis and enhanced magnetic, photocatalytic properties of one-dimensional Ag@Fe₃O₄-TiO₂. *Appl Surf Sci* 392:268–276
- Venkatachalam N, Palanichamy M, Murugesan V (2007) Sol-gel preparation and characterization of alkaline earth metal doped nano TiO₂: efficient photocatalytic degradation of 4-chlorophenol. *J Mol Catal A Chem* 273:177–185
- Teh CM, Mohamed AR (2010) Roles of titanium dioxide and ion-doped titanium dioxide on photocatalytic degradation of organic pollutants (phenolic compounds and dyes) in aqueous solutions: a review. *J Alloys Compd* 509:1648–1660
- Cheng Y, Sun H, Jin W, Xu N (2007) Photocatalytic degradation of 4-chlorophenol with combustion synthesized TiO₂ under visible light irradiation. *Chem Eng J* 128:127–133
- Choi J, Chung S, Cho K, Baek K, Hong S, Kim D, Lee S (2012) Photocatalytic degradation of chlorophenol compounds using poly aromatic star copolymer. *Water Air Soil Pollut* 223(3):1437–1441
- Fàbrega C, Andreu T, Cabot A, Ramon J (2010) Location and catalytic role of iron species in TiO₂: Fe photocatalysts: an EPR study. *J Photochem Photobiol A Chem* 211:170–175
- Zhang Q, Meng G, Wu J, Li D, Liu Z (2015) Study on enhanced photocatalytic activity of magnetically recoverable Fe₃O₄@C@TiO₂ nanocomposites with core-shell nanostructure. *Opt Mater* 46:52–58
- Wang JL, Xu LJ (2012) Advanced oxidation processes for wastewater treatment: formation of hydroxyl radical and application. *Crit Rev Environ Sci Technol* 42:251–325
- Han C, Zhang N, Xu YJ (2016) Structural diversity of graphene materials and their multifarious roles in heterogeneous photocatalysis. *Nano Today* 11:351–372
- Wang H, Wan W (2016) Synthesis of Fe₃O₄/N-TiO₂/Ag hollow nanospheres and their application as recyclable photocatalysts. *J Clust Sci* 27:403–415
- Zhang N, Yang MQ, Liu S, Sun Y, Xu YJ (2015) Waltzing with the versatile platform of graphene to synthesize composite photocatalysts. *Chem Rev* 115:10307–10377
- Zhao Y, Tao C, Xiao G, Wei G, Li L, Liu C, Su H (2016) Controlled synthesis and photocatalysis of sea urchin-like Fe₃O₄@TiO₂@Ag nanocomposites. *Nanoscale* 8:5313–5326
- Zhu J, Ren J, Huo Y, Bian Z, Li H (2010) Nanocrystalline Fe/TiO₂ visible photocatalyst with a mesoporous structure prepared via a nonhydrolytic sol-gel route. *J Phys Chem C* 111:18965–18969
- Mahmiani Y, Sevim AM, Gül A (2016) Photocatalytic degradation of 4-chlorophenol under visible light by using TiO₂ catalysts impregnated with Co (II) and Zn (II) phthalocyanine derivatives. *J Photochem Photobiol A Chem* 321:24–32
- Yang MQ, Zhang N, Wang Y, Xu YJ (2017) Metal-free, robust, and regenerable 3D graphene-organics aerogel with high and stable photosensitization efficiency. *J Catal* 346:21–29
- Akpan UG, Hameed BH (2009) Parameters affecting the photocatalytic degradation of dyes using TiO₂-based photocatalysts: a review. *J Hazard Mater* 170:520–529
- Jamalluddin NA, Abdullah AZ (2011) Reactive dye degradation by combined Fe(III)/TiO₂ catalyst and ultrasonic irradiation: effect of Fe(III) loading and calcination temperature. *Ultrason Sonochem* 18:669–678
- Nguyen VN, Nguyen NKT, Nguyen PH (2011) Hydrothermal synthesis of Fe-doped TiO₂ nanostructure photocatalyst. *Adv Nat Sci Nanosci Nanotechnol* 2:035014
- Kim HJ, Jeong KJ, Bae DS (2012) Synthesis and characterization of Fe doped TiO₂ nanoparticles by a sol-gel and hydrothermal process. *Korean J Mater Res* 22:249–252
- Paola AD, Marci G, Palmisano L, Schiavello M, Uosaki K, Ikeda S, Ohtani B (2002) Preparation of polycrystalline TiO₂ photocatalysts impregnated with various transition metal ions: characterization and photocatalytic activity for the degradation of 4-nitrophenol. *J Phys Chem B* 106:637–645
- Cong Y, Zhang J, Chen F, Anpo M, He D (2007) Preparation, photocatalytic activity, and mechanism of nano-TiO₂ co-doped with nitrogen and iron (III). *J Phys Chem C* 111:10618–10623
- Zhu J, Zheng W, He B, Zhang J, Anpo M (2004) Characterization of Fe-TiO₂ photocatalysts synthesized by hydrothermal method and their photocatalytic reactivity for photodegradation of XRG dye diluted in water. *J Mol Catal A Chem* 216:35–43
- Tong T, Zhang J, Tian B, Chen F, He D (2008) Preparation of Fe³⁺-doped TiO₂ catalysts by controlled hydrolysis of titanium alkoxide and study on their photocatalytic activity for methyl orange degradation. *J Hazard Mater* 155:572–579
- Pomogailo AD, Dzhardimalieva GI (2014) Thermolysis of metallopolymers and their precursors as a way for synthesis of nanocomposites. *Nanostructured materials preparation via condensation ways*. Springer, Berlin, pp 287–388
- Xu L, Wang J (2012) Fenton-like degradation of 2,4-dichlorophenol using Fe₃O₄ magnetic nanoparticles. *Appl Catal B Environ* 123–124:117–126
- Kim SE, Woo JY, Kang SY, Min BK, Lee JK, Lee SW (2016) A Facile general route for ternary Fe₂O₃@TiO₂@nanometal (Au, Ag) composite as a high-performance and recyclable photocatalyst. *J Ind Eng Chem* 43:142–149
- Xu L, Wang J (2012) Magnetic nanoscaled Fe₃O₄/CeO₂ composite as an efficient fenton-like heterogeneous catalyst for degradation of 4-chlorophenol. *Environ Sci Technol* 46:10145–10153
- Li HP, Liu JY, Liang XF, Hou WG, Tao XT (2014) Enhanced visible light photocatalytic activity of bismuth oxybromide lamellas with decreasing lamella thicknesses. *J Mater Chem A* 2:8926–8932
- Jeong ED, Borse PH, Jang JS, Lee JS, Jung O, Chang H, Jin JS, Won MS, Kim HG (2008) Hydrothermal synthesis of Cr and Fe co-doped TiO₂ nanoparticle photocatalyst. *J Ceram Process Res* 9:250–253
- Sood S, Umar A, Kumar S, Kumar S (2015) Highly effective Fe-doped TiO₂ nanoparticles photocatalysts for visible-light driven photocatalytic degradation of toxic organic compounds. *J Colloid Interface Sci* 450:213–223
- Hamad HA, Sadik WA, El-latif MMA, Kashyout AB, Feteha MY (2016) Photocatalytic parameters and kinetic study for degradation of dichlorophenol-indophenol (DCPIP) dye using highly active mesoporous TiO₂ nanoparticles. *J Environ Sci* 43:26–39
- Huerta Aguilar CA, Pandiyan T, Arenas-Alatorre JA, Singh N (2015) Oxidation of phenols by TiO₂Fe₃O₄M (M = Ag or Au) hybrid composites under visible light. *Sep Purif Technol* 149:265–278
- Surolia PK, Tayade RJ, Jasra RV (2007) Effect of anions on the photocatalytic activity of Fe(III) salts impregnated TiO₂. *Ind Eng Chem Res* 46:6196–6203
- Lo SM, Gilpavas E, Bojarska J, Kozanecki M, Rynkowski JM (2015) Transition metal loaded TiO₂ for phenol photo-degradation. *C R Chim* 18:1170–1182
- Shojaie A, Fattahi M, Jorfi S, Ghasemi B (2017) Hydrothermal synthesis of Fe-TiO₂-Ag nano-sphere for photocatalytic degradation of 4-chlorophenol (4-CP): investigating the effect of hydrothermal temperature and time as well as calcination temperature. *J Environ Chem Eng* 5:4564–4572
- Payan A, Fattahi M, Jorfi S, Roozbehani B, Payan S (2018) Synthesis and characterization of titanate nanotube/single-walled carbon nanotube (TNT/SWCNT) porous nanocomposite and its

- photocatalytic activity on 4-chlorophenol degradation under UV and solar irradiation. *Appl Surf Sci* 434:336–350
41. Busiakiewicz A, Kisielewska A, Piwoński I, Batory D (2017) The effect of Fe segregation on the photocatalytic growth of Ag nanoparticles on rutile TiO₂(001). *Appl Surf Sci* 401:378–384
 42. Brillas E, Martínez-Huitle CA (2015) Decontamination of wastewaters containing synthetic organic dyes by electrochemical methods. An updated review. *Appl Catal B Environ* 166–167:603–643
 43. Li H, Yin S, Wang Y, Sato T (2013) Efficient persistent photocatalytic decomposition of nitrogen monoxide over a fluorescence-assisted CaAl₂O₄:(Eu, Nd)/(Ta, N)-codoped TiO₂/Fe₂O₃. *Appl Catal B Environ* 132–133:487–492
 44. Li S, Xu Y, Wang X, Guo Y, Mu Q (2016) Catalytic degradation of 4-chlorophenol with La/TiO₂ in a dielectric barrier discharge system. *RSC Adv* 6:28994–29002
 45. Li X, Cabbage JW, Tetzlaff TA, Jenks WS (1999) Photocatalytic degradation of 4-chlorophenol. 1. The hydroquinone pathway. *J Org Chem* 64:8509–8524
 46. Li X, Cabbage JW, Jenks WS (1999) Photocatalytic degradation of 4-chlorophenol. 2. The 4-chlorocatechol pathway. *J Org Chem* 64:8525–8536
 47. Zhang Y, Wang T, Zhou M, Wang Y, Zhang Z (2017) Hydrothermal preparation of Ag-TiO₂ nanostructures with exposed {001}/ {101} facets for enhancing visible light photocatalytic activity. *Ceram Int* 43:3118–3126
 48. Hussain ST, Siddiq A (2011) Iron and chromium doped titanium dioxide nanotubes for the degradation of environmental and industrial pollutants. *Int J Environ Sci Technol* 8:351–362
 49. Guo JF, Ma B, Yin A, Fan K, Dai WL (2011) Photodegradation of rhodamine B and 4-chlorophenol using plasmonic photocatalyst of Ag-AgI/Fe₃O₄@SiO₂ magnetic nanoparticle under visible light irradiation. *Appl Catal B Environ* 101:580–586
 50. Mousavi-Mortazavi S, Nezamzadeh-Ejehieh A (2016) Supported iron oxide onto an Iranian clinoptilolite as a heterogeneous catalyst for photodegradation of furfural in a wastewater sample. *Desalin Water Treat* 57:10802–10814
 51. Zhang Y, Wu H, Zhang J, Wang H, Lu W (2012) Enhanced photodegradation of pentachlorophenol by single and mixed cationic and nonionic surfactants. *J Hazard Mater* 221–222:92–99
 52. Liu Y, Liu Y, Yang Z, Wang J (2017) Fenton degradation of 4-chlorophenol using H₂O₂ in situ generated by Zn-CNTs/O₂ system. *RSC Adv* 7:49985–49994
 53. Sobana N, Swaminathan M (2007) The effect of operational parameters on the photocatalytic degradation of acid red 18 by ZnO. *Sep Purif Technol* 56:101–107

Publisher's Note Springer Nature remains neutral with regard to jurisdictional claims in published maps and institutional affiliations.

